Rapid Communications

Self-modulation doping effect in the high-mobility layered semiconductor Bi_2O_2Se

Huixia Fu,[1] Jinxiong Wu,[2] Hailin Peng,[2] and Binghai Yan[1,*]

[1]*Department of Condensed Matter Physics, Weizmann Institute of Science, Rehovot 7610001, Israel*

[2]*Center for Nanochemistry, Beijing Sciences and Engineering Centre for Nanocarbons, College of Chemistry and Molecular Engineering, Peking University, Beijing 100871, China*

(Received 28 March 2018; revised manuscript received 11 June 2018; published 25 June 2018)

Recently, an air-stable layered semiconductor Bi_2O_2Se was discovered to exhibit an ultrahigh mobility in transistors fabricated with its thin layers. In this work, we explored the mechanism that induces the high mobility and distinguishes Bi_2O_2Se from other semiconductors. We found that the electron donor states lie above the lowest conduction band. Thus, electrons get spontaneously ionized from donor sites (e.g., Se vacancies) without involving the thermal activation, different from the donor ionization in conventional semiconductors. Consequently, the resistance decreases as reducing the temperature as observed in our measurement, which is similar to a metal but contrasts to a usual semiconductor. Furthermore, the electron conduction channels locate spatially away from ionized donor defects (Se vacancies) in different van der Waals layers. Such a spatial separation can strongly suppress the scattering caused by donor sites and subsequently increase the electron mobility, especially at the low temperature. We call this high-mobility mechanism self-modulation doping, i.e., the modulation doping spontaneously happening in a single-phase material without requiring a heterojunction. Our work paves a way to design high-mobility semiconductors with layered materials.

DOI: 10.1103/PhysRevB.97.241203

High-mobility devices and materials are significant for both fundamental research and semiconductor technology. A well-known method to realize the high mobility is the modulation doping based on a heterostructure that spatially separates carrier from ionized impurities [1]. This mechanism was also theoretically proposed to design highly conductive semiconductor nanowires recently [2,3]. In recent years, two-dimensional (2D) materials including graphene [4–9] and three-dimensional topological semimetals [10,11] provide new high-mobility platforms with ultrafast Dirac electrons. Very recently, an emerging layered semiconductor, bismuth oxychalcogenide (Bi_2O_2Se), was found to exhibit ultrahigh electron mobility and strong quantum oscillations in fabricated devices [12]. Soon this material was fabricated into ultrafast, highly sensitive infrared photodetectors [13] and magnetoresistance devices [14], and was predicted to be a candidate for the ferroelectric property [15].

The Bi_2O_2Se compound attracts great research attention for designing novel devices, while the fundamental origin of its high mobility remains unexplored. Similar layered chalcogenides, such as the well-known topological insulator [16,17] Bi_2Se_3, usually suffer from the self-doping (e.g., Se vacancies) and exhibit very low mobility [18–20]. Furthermore, the resistance of a usual semiconductor decreases on increasing the temperature [21], because free carriers require the thermal energy to get ionized from donor/acceptor sites. In contrast, the resistance of Bi_2O_2Se exhibits an opposite trend to the temperature [12,22]. In addition, such a temperature dependence of the resistance is reminiscent of a similar trend observed in $SrTiO_3$ [23,24]. The uniqueness of this material motivates us to investigate its electronic structure to understand its transport properties.

In ordinary semiconductors, it is known as the defect states are normally located in the band gap and lower than the empty conduction bands as shown in Fig. 1(a). In order to achieve the conducting channels, the excess electrons should be excited to the next conduction band by temperature. Free electrons display the higher density at a higher temperature and thus, the resistance will decrease sharply with increasing temperature. In contrast, Bi_2O_2Se samples exhibit a different *R-T* dependence from ordinary semiconductors [see Fig. 1(b)].

In this Rapid Communication, we have performed experimental and theoretical studies on the electronic and transport properties of Bi_2O_2Se. We have found that Se vacancies (V_{Se}) and Se-Bi antisites (Se_{Bi}) are crucial donors for electron carriers in this material. Because the V_{Se} distributes in the Se layer while the wave function of conduction electrons locates in the Bi_2O_2 layer in the lattice, the scattering of V_{Se} to electron carriers is much weaker. However, Se_{Bi} scatters electrons strongly, since it distributes in the same Bi_2O_2 layer as the conduction band [Fig. 1(c)]. Interestingly, as evidenced by the formation energy calculations, the relative amount of V_{Se} and Se_{Bi} can be readily adjusted by changing the Se richness during synthesis. V_{Se} is the major defect in the Se-poor condition while Se_{Bi} is the major one in the Se-rich condition, which well explained the low-temperature mobility variation of Bi_2O_2Se synthesized under different Se-richness conditions. Further, we found that the donor levels of both V_{Se} and Se_{Bi} lie above the conduction-band bottom in energy by calculations. Such a band structure induces the automatic ionization of free electrons from these defects without overcoming an activation barrier [Fig. 1(b)]. It explains the metal-like temperature dependence of the resistance measured.

*binghai.yan@weizmann.ac.il

 ©2018 American Physical Society

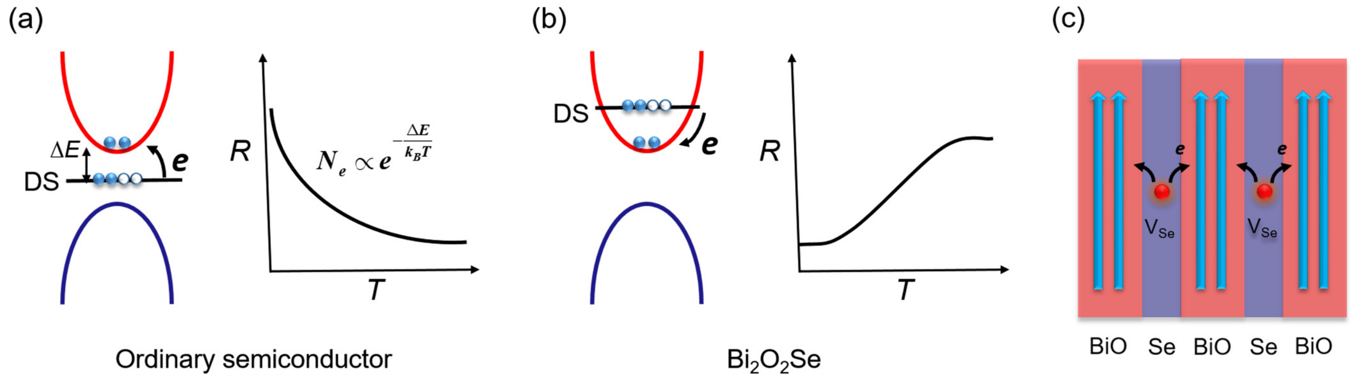

FIG. 1. Energy level for defect state (DS), electron-doping process, and temperature-dependent resistance for ordinary semiconductors (a) and Bi_2O_2Se (b). (c) Diagram of spatial separation between conducting channels and donor vacancies (V_{Se}) in Bi_2O_2Se.

In the Se-richness-controlled chemical vapor deposition growth experiments [29], we found there are two types of 2D Bi_2O_2Se samples with obviously distinct transport performances under different Se-richness growth conditions. The Se/Bi ratio is controlled by adjusting the ratio of Bi_2Se_3 and Bi_2O_3 that were used as coevaporation sources (i.e., keep the amount of Bi_2O_3 constant, while changing the amount of Bi_2Se_3 independently). As shown in Figs. 2(a) and 2(b), both the Se-poor and Se-rich samples show a metal-like R-T behavior, namely, longitudinal resistance (R_{xx}) decreases monotonously upon cooling down. This R-T feature is different from the ordinary semiconductor, whose resistance usually increases sharply upon cooling down [see Fig. 1(a), for example]. Remarkably, the Bi_2O_2Se samples synthesized under different Se richness show significant differences on residual resistance ratio (RRR, defined as $R_{xx,\,300\,K}/R_{xx,\,2\,K}$), which is a key parameter to reflect the intrinsic quality of samples obtained. As shown in Figs. 2(a) and 2(b), the typical RRR of Se-poor Bi_2O_2Se (67.6) is about an order of magnitude higher than the Se-rich one (7.2). A higher RRR usually indicates a higher Hall mobility. Figures 2(c) and 2(d) show the evolution of Hall mobility and carrier density

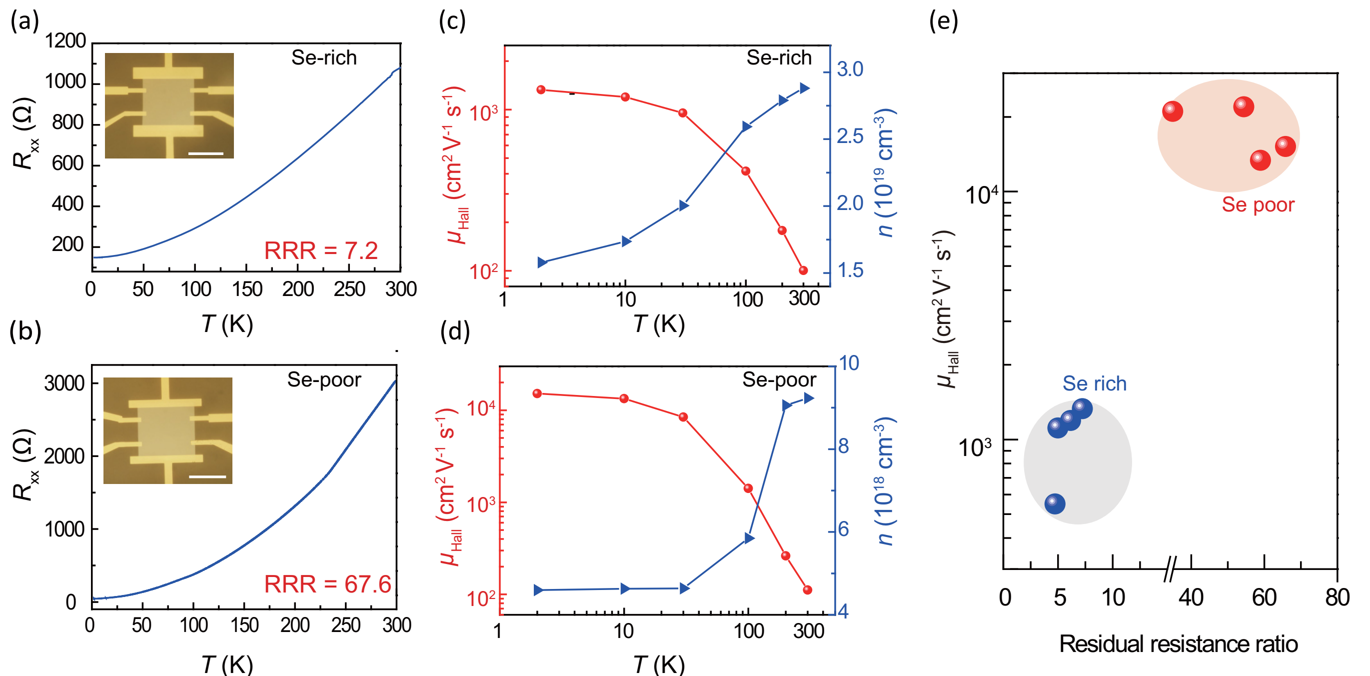

FIG. 2. Electrical measurements of 2D Bi_2O_2Se crystals synthesized under different Se-richness growth conditions. (a), (b) Typical temperature-dependence longitudinal resistance (R_{xx}) of 2D Bi_2O_2Se crystals synthesized under relatively Se-rich (a) and Se-poor (b) conditions, showing significant difference on residual resistance ratios (RRRs). The Se richness is controlled by adjusting the ratio of Bi_2Se_3 and Bi_2O_3 that were used as coevaporation sources (i.e., keep the amount of Bi_2O_3 constant, while changing the amount of Bi_2Se_3 independently). Inset: optical microscope images of Bi_2O_2Se Hall-bar devices fabricated on mica substrate. Both Bi_2O_2Se devices have a similar thickness of 10 nm. Scale bar: 50 μm. (c), (d) The corresponding temperature-dependence Hall mobility (μ_{Hall}) and carrier density (n) of 2D Bi_2O_2Se crystals synthesized under relatively Se-rich (c) and Se-poor (d) conditions. (e) Statistics for low-temperature Hall mobility (2 K) and residual resistance ratios of 2D Bi_2O_2Se crystals synthesized under different Se-richness growth condition. Much higher Hall mobility and residual resistance ratio were obtained on Bi_2O_2Se crystals synthesized under a relatively Se-poor condition.

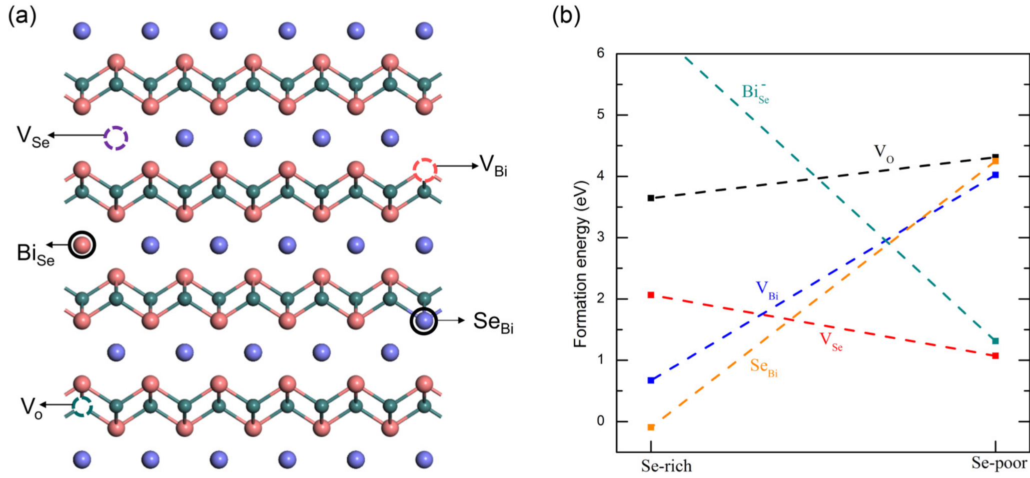

FIG. 3. (a) Atomic structure of Bi_2O_2Se with five possible defects. (b) The formation energy for these defects with respect to the chemical potential at different Se-richness conditions.

as a function of temperature. The Hall mobility (μ_{Hall}) is obtained from $\mu_{\mathrm{Hall}} = (L/W)(G/ne)$, where e is the charge of an electron and n is the 2D charge density determined from Hall coefficient R_{H} measurements ($n = 1/eR_{\mathrm{H}}$). Remarkably, the Hall mobility of both Se-rich and Se-poor samples increased monotonously as the temperature cools downs to 2 K, and this feature fits well with a phonon-dominated charge transport mechanism. Interestingly, the Se-poor sample holds a significantly higher Hall mobility ($>$15 000 $\mathrm{cm^2\,V^{-1}\,s^{-1}}$) than the Se-poor sample ($\sim$1000 $\mathrm{cm^2\,V^{-1}\,s^{-1}}$) at 2 K, while showing a similar room-temperature Hall mobility. It can be well explained by taking into consideration that the charge impurities (defects) scattering usually dominate the scattering events at low temperature, while phonon scattering dominates at room temperature [25–27]. In other words, our experimental results suggest, to some extent, the existence of some kinds of defects that may greatly depress the mobility of Se-rich Bi_2O_2Se. To further confirm this feature, we performed the statistics for low-temperature Hall mobility (2 K) and residual resistance ratios of 2D Bi_2O_2Se crystals synthesized under different Se-richness growth condition [Fig. 2(e)]. Obviously, the Se-poor samples indeed show much higher mobility and residual resistance ratio than the Se-rich one.

To understand the origin of unusual resistance behavior and the high mobility, we have performed first-principles calculations [28] to explore the structural and electronic properties of Bi_2O_2Se in the following. We first estimate the formation of possible defects as potential donors and acceptors with respect to the experimental condition. The free carriers in Bi_2O_2Se are expected to come from lattice defects, since there are no specific impurities introduced in the experiment. As shown by the atomic configuration displayed in Fig. 3(a), Bi_2O_2Se exhibits a layered crystal structure consisting of alternate Bi_2O_2 layers and Se layers. The Bi-Se distance in Bi_2O_2Se is 3.28 Å, longer than the strong covalent bond length of 2.84–3.05 Å in Bi_2Se_3. This suggests that the Bi_2O_2 and Se layers are combined with relatively weak electrostatic interaction. Five possible defects are considered here: Se vacancies (V_{Se}), Bi vacancies (V_{Bi}), O vacancies (V_{O}), Se antisites at Bi positions ($\mathrm{Se_{Bi}}$), and Bi antisites at Se positions ($\mathrm{Bi_{Se}}$), as illustrated in Fig. 3(a). The defect formation energies are calculated for the Se-rich and Se-poor conditions, as displayed in Fig. 3(b). The chemical potential of the Se element at the Se-rich limit refers to the one in bulk Se, while the chemical potential of Se in Bi_2Se_3 is taken into consideration for the Se-poor limit [29]. Among the five types of defects, V_{Se} and $\mathrm{Se_{Bi}}$ present the lowest formation energies at the Se-poor and Se-rich conditions, respectively. This indicates that V_{Se} and $\mathrm{Se_{Bi}}$ are probably the dominant defects in general. Because of the large slope of the $\mathrm{Se_{Bi}}$ formation energy [Fig. 3(b)], the existence of $\mathrm{Se_{Bi}}$ is expected to be strongly suppressed in the Se-poor condition. In short, V_{Se} is the major defect in the Se-poor condition while $\mathrm{Se_{Bi}}$ is the major one in the Se-rich condition.

Next, we investigate the roles of V_{Se} and $\mathrm{Se_{Bi}}$ in doping the semiconductor Bi_2O_2Se. Figure 4 shows band structures of the pristine bulk and those with V_{Se} and $\mathrm{Se_{Bi}}$ defects. We choose a $5 \times 5 \times 2$ bulk supercell that contains 500 atoms to simulate the doping effect of a single defect, to suppress the interaction of defects from neighboringd supercells. The pristine bulk presents an energy gap. The existence of both V_{Se} and $\mathrm{Se_{Bi}}$ shift the Fermi energy up into the conduction bands. In contrast to the doping effect of a conventional semiconductor [illustrated in Fig. 1(a)], both defects do not induce any in-gap donor states in the band structure. Corresponding donor states lie about 0.8 eV above the conduction-band bottom. Each V_{Se} ($\mathrm{Se_{Bi}}$) site donates two (one) electrons to the bulk, consistent with the shifted Fermi energy position. In addition, we note that the 0.32 eV indirect gap of Bi_2O_2Se is underestimated by the density-functional theory (DFT). But the positions of V_{Se} and $\mathrm{Se_{Bi}}$ with respect to the conduction band are not affected by the DFT band gap. Similarly, V_{Bi} and V_{O} are found to be acceptors with acceptor levels in the valence bands [29]. The fact that V_{Se} and $\mathrm{Se_{Bi}}$ are dominant for different Se richness indicates corresponding samples are electron doped, well consistent with our experimental observation.

Because the donor states caused by V_{Se} and $\mathrm{Se_{Bi}}$ are higher in energy than the conduction-band bottom, excess electrons spontaneously move from donor states to the conduction band without requiring thermal activation. Therefore, the resultant electron carrier density does not increase exponentially with

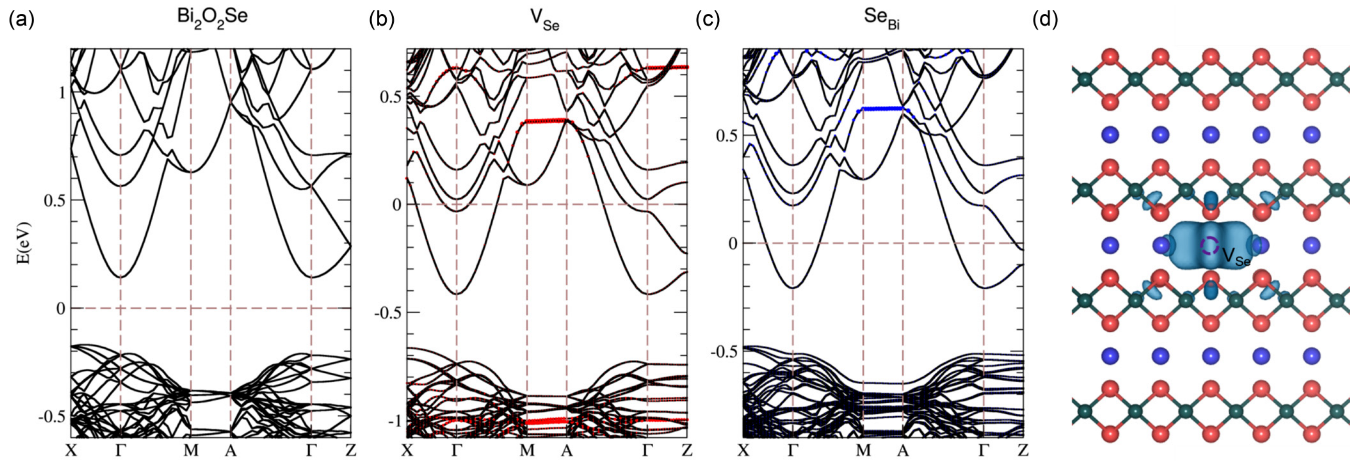

FIG. 4. Calculated band structures of (a) perfect Bi_2O_2Se and the configurations with domain defects (b) V_{Se} and (c) Se_{Bi} antisite. Fermi level is set at 0. In (b), the red and blue dots, respectively, present the projected bands on the nearest neighbor Bi and Se atoms close to the V_{Se}. In (c), the blue dots denote the states located on the Se atom which is on a site previously occupied by a Bi atom. (d) The charge density distribution for the V_{Se} defect state marked by the filled purple circle in (b) at the M k point. The isosurface of the charge density corresponds to 0.0015 $e/\text{Å}^3$.

increasing temperature, i.e., $N_e \propto e^{-\Delta E/k_BT}$, where ΔE is the activation energy. Instead, the carrier density shows weak dependence on the temperature. It is consistent with the fact that the carrier density remains in the same order of magnitude from 2 to 300 K, for both Se-rich and Se-poor samples [see Figs. 2(b) and 2(d)]. Further, it also well explains that R_{xx}-T behavior of Bi_2O_2Se is similar to a metal rather than a semiconductor. With reducing the temperature, the decreasing resistance is mainly caused by the quickly increasing mobility.

Additionally, we can rationalize the high energy of the V_{Se} state in the band structure by some chemical intuition. The Bi_2O_2Se lattice can be viewed as stacking Se^{2-} and $(Bi_2O_2)^{2+}$ layers alternatively. The Se^{2-} and $(Bi_2O_2)^{2+}$ layers bind together by ionic-like bonds, different from an ordinary covalent semiconductor. It is hard for the V_{Se} to trap a free electron because of the strong electrostatic repulsion inside the negative-charge-carried Se^{2-} layer. This leads to the much higher energy of the vacancy level as revealed by our calculations.

Furthermore, we discuss different roles of V_{Se} and Se_{Bi} in the electron mobility. Recall that the wave function of the lowest conduction band distributes predominantly inside the Bi_2O_2 layer; V_{Se} defect states that locate in the Se layer [see Fig. 4(d)] are spatially separated from the conducting electrons. Consequently, the scattering due to the ionized donor sites is suppressed, giving rise to the large mobility at low temperature. Here, the separation of donor sites and free electrons are naturally realized in a single-phase material, leading to the same effect as the modulation doping. Thus, we refer to the high-mobility mechanism in Bi_2O_2Se as the self-modulation doping. For the other donor Se_{Bi}, the conducting channels are strongly disrupted because Se_{Bi} sites locate inside the same Bi_2O_2 layers, inducing much lower mobility than the V_{Se} case. Therefore, the spatial distribution of two defects explains the large mobility variation between samples from the Se-poor (V_{Se}-dominated, high-mobility) and Se-rich (Se_{Bi}-dominated, low-mobility) conditions. In addition, we should note that the 2D layered structure is the precondition for the large separation of conduction electrons and the ionized defects. It is different from the case of the three-dimensional material $SrTiO_3$.

In conclusion, combing the experimental measurements and first-principles calculations, we have found that the self-modulation doping mechanism in the layered Bi_2O_2Se semiconductor leads to the high electron mobility. Our work also explains the unusual metal-like resistance-temperature dependence of Bi_2O_2Se. Our findings pave a way to design high-mobility semiconductors in emerging layered materials.

B.H.Y. is supported by a research grant from the Benoziyo Endowment Fund for the Advancement of Science. H.L.P. and J.X.W. acknowledge financial support from the National Basic Research Program of China (Grants No. 2014CB932500, No. 2016YFA0200101, and No. 2014CB920900), the National Natural Science Foundation of China (Grants No. 21733001, No. 21525310, and No. 11774010), and a China Postdoctoral Science Foundation funded project.

H.F. and J.W. contributed equally to this work.

[1] R. Dingle, H. L. Störmer, A. C. Gossard, and W. Wiegmann, Electron mobilities in modulation-doped semiconductor heterojunction superlattices, Appl. Phys. Lett. **33**, 665 (1978).

[2] B. Yan, G. Zhou, X. C. Zeng, J. Wu, B.-L. Gu, and W. Duan, Quantum confinement of crystalline silicon nanotubes with nonuniform wall thickness: Implication to modulation doping, Appl. Phys. Lett. **91**, 103107 (2007).

[3] B. Yan, T. Frauenheim, and Á. Gali, Gate-controlled donor activation in silicon nanowires, Nano Lett. **10**, 3791 (2010).
[4] K. S. Novoselov, A. K. Geim, S. V. Morozov, D. Jiang, M. I. Katsnelson, I. V. Grigorieva, S. V. Dubonos, and A. A. Firsov, Two-dimensional gas of massless Dirac fermions in graphene, Nature (London) **438**, 197 (2005).
[5] W. Zhang, Z. Huang, W. Zhang, and Y. Li, Two-dimensional semiconductors with possible high room temperature mobility, Nano Res. **7**, 1731 (2014).
[6] S. Das, H.-Y. Chen, A. V. Penumatcha, and J. Appenzeller, High performance multilayer MoS_2 transistors with scandium contacts, Nano Lett. **13**, 100 (2012).
[7] H. Liu, A. T. Neal, Z. Zhu, Z. Luo, X. Xu, D. Tománek, and P. D. Ye, Phosphorene: An unexplored 2D semiconductor with a high hole mobility, ACS Nano **8**, 4033 (2014).
[8] J. Qiao, X. Kong, Z. X. Hu, F. Yang, and W. Ji, High-mobility transport anisotropy and linear dichroism in few-layer black phosphorus, Nat. Commun. **5**, 4475 (2014).
[9] J. Kim, S. S. Baik, S. H. Ryu, Y. Sohn, S. Park, B.-G. Park, J. Denlinger, Y. Yi, H. J. Choi, and K. S. Kim, Observation of tunable band gap and anisotropic Dirac semimetal state in black phosphorus, Science **349**, 723 (2015).
[10] T. Liang, Q. Gibson, M. N. Ali, R. J. Cava, and N. P. Ong, Ultrahigh mobility and giant magnetoresistance in the Dirac semimetal Cd_3As_2, Nat. Mater. **14**, 280 (2015).
[11] C. Shekhar, A. K. Nayak, Y. Sun, Y. M. Schmidt, M. Nicklas, I. Leermakers, U. Zeitler, Y. Skourski, J. Wonsnitza, Z. Liu *et al.*, Extremely large magnetoresistance and ultrahigh mobility in the topological Weyl semimetal candidate NbP, Nat. Phys. **11**, 645 (2015).
[12] J. Wu, H. Yuan, M. M. Meng, C. Chen, Y. Sun, Z. Chen, W. Dang, C. Tan, Y. Liu, J. Yin *et al.*, High electron mobility and quantum oscillations in non-encapsulated ultrathin semiconducting Bi_2O_2Se, Nat. Nanotechnol. **12**, 530 (2017).
[13] J. Yin, Z. Tan, H. Hong, J. Wu, H. Yuan, Y. Liu, C. Chen, C. Tan, F. Yao, Y. Chen *et al.*, Ultrafast, highly-sensitive infrared photodetectors based on two-dimensional oxyselenide crystals, arXiv:1712.05942.
[14] M. Meng, S. Huang, C. Tan, J. Wu, Y. Jing, H. Peng, and H. Q. Xu, Strong spin-orbit interaction and magnetotransport in semiconductor Bi_2O_2Se nanoplates, Nanoscale **10**, 2704 (2018).
[15] M. Wu and X. C. Zeng, Bismuth oxychalcogenides: A new class of ferroelectric/ferroelastic materials with ultra high mobility, Nano Lett. **17**, 6309 (2017).
[16] M. Z. Hasan and C. L. Kane, Colloquium: Topological insulators, Rev. Mod. Phys. **82**, 3045 (2010).
[17] X. L. Qi and S. C. Zhang, Topological insulators and superconductors, Rev. Mod. Phys. **83**, 1057 (2011).
[18] A. A. Taskin, S. Sasaki, K. Segawa, and Y. Ando, Manifestation of Topological Protection in Transport Properties of Epitaxial Bi_2Se_3 Thin Films, Phys. Rev. Lett. **109**, 066803 (2012).
[19] D. Kim, S. Cho, N. P. Butch, P. Syers, K. Kirshenbaum, S. Adam, J. Paglione, and M. S. Fuhrer, Surface conduction of topological Dirac electrons in bulk insulating Bi_2Se_3, Nat. Phys. **8**, 459 (2012).
[20] A. A. Taskin, S. Sasaki, K. Segawa, and Y. Ando, Achieving surface quantum oscillations in topological insulator thin films of Bi_2Se_3, Adv. Mater. **24**, 5581 (2012).
[21] C. D. Thurmond, The standard thermodynamic functions for the formation of electrons and holes in Ge, Si, GaAs, and GaP, J. Electrochem. Soc. **122**, 1133 (1975).
[22] J. Wu, C. Tan, Z. Tan, Y. Liu, J. Yin, W. Dang, M. Wang, and H. Peng, Controlled synthesis of high-mobility atomically thin bismuth oxyselenide crystals, Nano Lett. **17**, 3021 (2017).
[23] O. N. Tufte and P. W. Chapman, Electron mobility in semiconducting strontium titanate, Phys. Rev. **155**, 796 (1967).
[24] A. Spinelli, M. A. Torija, C. Liu, C. Jan, and C. Leighton, Electronic transport in doped $SrTiO_3$: Conduction mechanisms and potential applications, Phys. Rev. B **81**, 155110 (2010).
[25] B. Radisavljevic and A. Kis, Mobility engineering and a metal–insulator transition in monolayer MoS_2, Nat. Mater. **12**, 815 (2013).
[26] L. Li, G. J. Ye, V. Tran, R. Fei, G. Chen, H. Wang, J. Wang, K. Watanabe, T. Taniguchi, L. Yang *et al.*, Quantum oscillations in a two-dimensional electron gas in black phosphorus thin films, Nat. Nanotechnol. **10**, 608 (2015).
[27] X. Cui, G. H. Lee, Y. D. Kim, G. Arefe, P. Y. Huang, C.-H. Lee, D. A. Chenet, X. Zhang, L. Wang, F. Ye *et al.*, Multi-terminal transport measurements of MoS_2 using a van der Waals heterostructure device platform, Nat. Nanotechnol. **10**, 534 (2015).
[28] G. Kresse and J. Furthmüller, Efficient iterative schemes for *ab initio* total-energy calculations using a plane-wave basis set, Phys. Rev. B **54**, 11169 (1996).
[29] See Supplemental Material at http://link.aps.org/supplemental/10.1103/PhysRevB.97.241203 for the DFT method, experimental method, structural characterizations, and formation energy calculations.